Photoinduced Band Gap Shift and Deep Levels in Luminescent Carbon Nanotubes

Paul Finnie* and Jacques Lefebvre

Institute for Microstructural Sciences, National Research Council Canada, Building M-50, 1200 Montreal Road, Ottawa, ON, Canada K1A 0R6

ABSTRACT

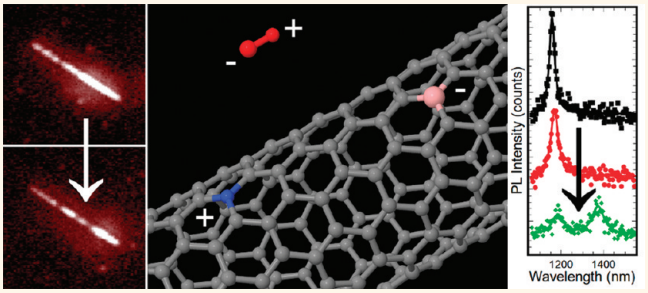

Individual air-suspended single-walled carbon nanotubes are imaged both spatially and spectrally in photoluminescence. At low excitation power, photoluminescence is bright and stable with high quantum efficiency; however, higher power initially causes a gradual red shift and then more severe changes. Blinking, the loss of quantum efficiency, and the appearance of new deep levels are all seen and can be explained by the introduction of defects. We propose that optical excitation induces molecular deposition onto the nanotube by optically induced van der Waals interactions, leading to physisorption and ultimately chemisorption which severely degrades the luminescence.

KEYWORDS: single-walled carbon nanotube · photoluminescence · exciton · quantum efficiency · band gap shift · van der Waals interaction

Single-walled carbon nanotubes (SWNTs) are the real world realizations of idealized one-dimensional materials, and their interactions with light are especially interesting and promising. Their unique properties suggest potential in optoelectronic applications, for example, as UV–vis–NIR light detectors, as tunable optical filters, and as NIR light sources, with the prospect of compatibility with inexpensive, large-scale printed processes. Recently, research in optical properties has shifted from investigations of intrinsic luminescent properties of pristine tubes toward the extrinsic effects which can transform them. Here, extrinsic behavior is photoinduced. Most, if not all, organic materials photodegrade, and while they are not strictly speaking organic (since they are purely carbon), nanotubes are also changed by illumination. This is important from a basic science point of view and because some devices, such as nanotube lasers, may operate in intense optical fields.

In this paper, we show how air-suspended single-walled carbon nanotubes are affected by the excitation intensity of visible light using single nanotube PL imaging spectroscopy. The choice of air-suspended SWNTs is important because they are probably the closest real world approximation to the theoretical ideal of pristine isolated nanotubes. Even so, nanotubes cannot be considered independently of their environment. We find that at very low excitation power densities the luminescence is photostable, has high quantum efficiency, and emission is concentrated in one principal wavelength (E_{11}). In air ambient, at slightly higher illumination intensities, we find that there is a small, gradual band gap red shift, followed by an onset of blinking, and reduction in quantum efficiency. With more intense or prolonged illumination, blinking becomes ever more vigorous, until the quantum efficiency collapses, bright deep levels are created, and the tube becomes much darker, typically becoming relatively photostable again at these lower brightness levels. We propose a picture in which light-induced physisorption is responsible for the red shift and light-induced chemisorption causes the blinking, loss of quantum efficiency, and deep level emission through the creation of defect sites. In this picture, photoexcited nanotubes are not simply passively changed by their environment, but rather they actively interact with the environment and are altered by it. Experimental details about sample preparation and PL imaging setup and measurement parameters are provided in the Methods section.

* Address correspondence to paul.finnie@nrc-cnrc.gc.ca.

Received for review December 1, 2011 and accepted January 27, 2012.

Published online February 06, 2012
10.1021/nn204679s

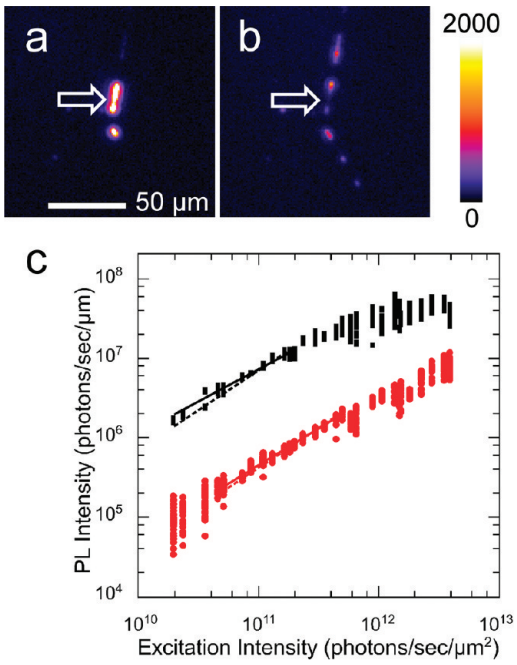

Figure 1. Laser illumination transforms a pristine SWNT into a damaged SWNT. (a) Bright suspended segments (arrow) of an individual long SWNT suspended over multiple segments of a quartz grating. Excitation was in the violet (405 nm) with a power with 1.4 mW incident on a 56 μm diameter spot, for a mean power density of 0.56 μW/μm^2 or 1.2 $\times$ 10^{12} photons/μm^2/s. The intensity scale is in counts. See Methods for conversion into photons. The integration time was 0.2 s. (b) Same region under similar conditions after exposure to 0.64 μW/μm^2 or 1.3 $\times$ 10^{12} photons/μm^2/s for approximately 3 min. The focus and spot position was adjusted slightly to try to maximize the signal from the photodamaged part. (c) PL intensity *versus* 405 nm laser power density for undamaged nanotube (black) *versus* the damaged nanotube (red). Data were taken with power increasing for both traces. The best fit linear scaling over a limited range is traced by a dotted line. The best fit power law over the same range is illustrated by the solid line.

RESULTS

Figure 1 shows how the excitation power affects the luminescence of a very bright nanotube. An isolated luminescent nanotube was found at an intermediate excitation power. The laser was blocked, and then the laser power swept from low excitation power to full power. Excitation was with a 405 nm laser, though we have observed similar effects at other wavelengths in air ambient. Each data point was integrated here for 200 ms, with each laser power sampled for several seconds. Figure 1a shows the segment at slightly reduced power, and though it has already sustained some damage at this point, it is still very bright. After the first sweep, the excitation was held at the fixed maximum power for approximately 3 min. During this time, the tube was blinking and visibly dimmed by almost 2 orders of magnitude. Then the laser power was swept as before. Figure 1b shows the same nanotube at the same power after the second sweep. The formerly very bright segment is barely visible. Some less damaged segments are visible at the edges of the spot where the laser intensity is lower. Although dark segments can sometimes become temporarily brighter, for example, through blinking, these segments are likely only visible because the laser spot, which has small spatial inhomogeneities, was adjusted prior to the second sweep.

Figure 1c shows how the integrated PL intensity evolved with laser power for a 5.3 μm long bright segment. The excitation power is given in photons/unit area, assuming uniform illumination in the spot. In fact, the spot is not uniform, and this actual power density at the tube could be somewhat lower (see Methods). The emission power is given in photons/unit length where we have plotted total (4π steradian) PL emission, where we have corrected with a factor for numerical aperture and instrumental response (see Methods for details).

At low excitation intensities, the PL intensity increases nearly linearly with excitation power density. The undamaged tube is shown in black. The dotted line is a linear fit, with best fit $y = (7.02 \pm 0.07) \times 10^{-5}x$, where x is power in photons/s/μm^2 and y is intensity in photons/s/μm. A slightly better fit can be obtained with a power law, with $y = (0.009 \pm 0.003)x^{0.81\pm0.01}$. Once the excitation intensity exceeds about 4 $\times$ 10^{11} photons/s/μm^2, the tube begins blinking dramatically, as can be seen by the increasingly wide scatter in brightness at high power. At the same time, there is a significant loss in quantum efficiency as the points deviate more and more from a straight line, dropping well below linearity. Plotting the brightness on a log scale like this tends to minimize the significance of the blinking. In terms of linear intensity, the blinking range from dimmest to brightest is approximately a factor of 5. It is important to note that this is actually a low excitation intensity from the point of view of many optical experiments such as point by point Raman or PL spectroscopy since often a tightly focused spot is used and certainly compared to pulsed excitation for dynamical studies. For reference, for a tightly focused 1 μm diameter spot, this threshold for blinking corresponds to less than 0.2 μW incident power. There are already some small fluctuations even at low power for the undamaged nanotube, and this is likely the consequence of the tube already suffering some damage due to light exposure before the sweep.

Blinking in nanotube fluorescence has recently seen a surge of interest. Blinking in short (~200 nm) micelle-encapsulated nanotubes on surfaces was seen early on[1,2] and has been attributed to charge trapping. Intensity fluctuations in some air-suspended nanotubes were also recognized early on in spatially resolved imaging of long nanotubes.[3] Blinking was induced for nanotubes in solution with acid treatments and recognized to have stepwise characteristics.[4] High intensity illumination was found to induce blinking in surface tubes and attributed to the creation of defect

states related to chemisorption of oxygen.[5,6] Stepwise blinking was found to occur for freely suspended nanotubes in oxygen ambient, but not in vacuum or in argon, and attributed to defect levels introduced by doping.[7] Capping layers were found to reduce blinking on surface nanotubes, presumably because they act as diffusion barriers.[8] Very recently, while this paper was under review, it was reported that elevated laser powers increase stepwise blinking frequency in micelle-encapsulated nanotubes.[9] Also very recently, relatively long (several micrometers) micelle-encapsulated nanotubes in solution have been imaged in photoluminescence while being chemically attacked to induce blinking. This enabled spatial and temporal correlations to be examined and interpreted in terms of adsorbate attachment−detachment-induced defects and their diffusion.[10]

Here, the postdamage sweep in red (Figure 1c) shows that 3 min exposure has reduced the tube brightness by a factor of almost 20×. After the damage, the PL intensity still scales linearly. The dotted red line is a linear fit, with best fit $y = (4.16 \pm 0.03) \times 10^{-6}x$, and an only marginally better fit is the solid red power law $y = (2.9 \pm 0.9) \times 10^{-5}x^{0.92\pm0.01}$ fit. The damaged tube still blinks at higher excitation powers and is also less stable at lower powers. In the linear regimes, the photodamaged tube is precisely 17× dimmer than the pristine tube. However, aside from being much dimmer and blinking more, it could easily be mistaken for a pristine nanotube.

The slope of the pristine curve necessarily implies a high quantum efficiency. With a 1 nm geometrical cross section, even supposing 4% absorption like a double layer of graphene at this wavelength,[11] a quantum efficiency of unity would give a slope 4×10^{-5} photons emitted/μm for photons incident on 1 μm^2, which is a little less than the measured value for the "pristine" tube in the linear regime. However, the nonuniformity in illumination is a large source of experimental error and should reduce the measured value (see the Methods for details). Previously, we rigorously estimated the quantum efficiency of air-suspended nanotubes at 7%; however, this estimate was made with conservative choices for the average excitation power, response of the system, and included "worst-case" reflection from the substrate.[3] Recent reports suggest solution-based nanotubes can have quantum efficiencies in the 10−30% range.[12,13] It is difficult to compare different quoted quantum efficiencies since they are deteremined using different methods, with different and not insignificant sources of error.

What can be said with certainty is that the damaged tube has much lower quantum efficiency than the intrinsic pristine nanotube, and many SWNT preparation approaches do cause significant damage. Ultrasonication, a common step in the production of nanotube solutions, is well-known to cause severe damage and even cuts nanotubes. If a tube is blinking at all, it would seem that it has already been damaged or doped. However, as can be seen from the red data at low excitation powers, a damaged nanotube can be

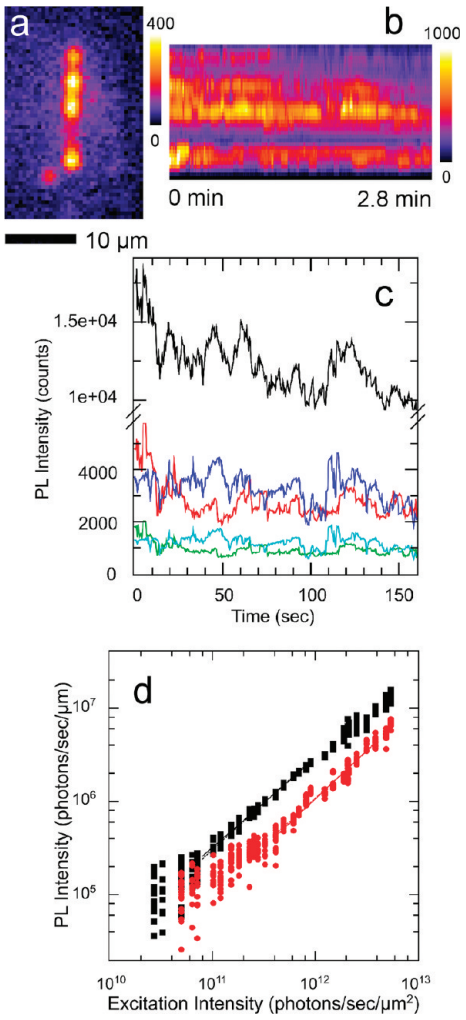

Figure 2. Blinking of a damaged SWNT. (a) Blinking suspended segments of an individual long SWNT suspended over multiple segments of a quartz grating viewed at an intermediate power, where it is relatively stable with 1.2 mW incident on a ~60 μm diameter spot. The intensity scale is in counts, and the integration time is 0.4 s. See Methods for conversion to photons. (b) Same region at 7.5 mW power tracked as a function of time over a period of almost 3 min. The vertical axis is the same spatial scale, while the horizontal axis shows the time evolution. (c) Graphs of the time evolution: black, the entire luminescent tube; red, entire bright segment at the bottom, 3.2 μm (6 pixels) long; blue, entire bright segment in the middle, 3.2 μm (6 pixels) long; green, a subset of the bright bottom segment, 1.1 μm (2 pixels) long; cyan, a subset of the middle bright segment, 1.1 μm (2 pixels) long. Stepwise quenching and brightening events can be easily discerned if the luminescent tube lengths are short. (d) PL intensity *versus* 405 nm laser power density for undamaged nanotube (black) *versus* the damaged nanotube (red). Data were taken with power decreasing in both traces. The best fit linear scaling over a limited range is traced by a dotted line, and the best power law fit is traced by a solid line; however, they are close together as to be indistinguishable on this scale.

fairly stable, so one might not easily recognize that a particular nanotube has been damaged. The idea that the quantum efficiency is low for nanotubes likely stems from the fact that most real nanotubes are doped or defective to a degree that alters their intrinsic properties and lowers the quantum efficiency.

The actual dynamics of the blinking here is fascinating. Figure 2 shows how a damaged tube blinks, and videos of blinking nanotubes are also provided in Supporting Information. This, a relatively weaker luminescent tube, was illuminated for 3 min after taking an initial laser power sweep, this time in decreasing intensity. Figure 2a shows the tube with the strongest illumination but still having relatively stable PL emission, before being seriously damaged. Several independently suspended segments are seen. Figure 2b shows how the intensity evolves as a function of time. The spatial axis is along the *y*-axis and has the same scale as panel a. The time axis is along the horizontal. Many intriguing effects can be seen. The tube blinks on and off locally. In some instances, the PL intensity appears to shift spatially up or down with bright regions becoming dark and dark regions becoming light, meaning that it does exhibit spatial correlations. The blinking, while not periodic, also does not appear random in time. In one unusual case, we observed an entire tube to blink repeatedly over 100 μm scales (see video in Supporting Information). Presumably such large-scale fluctuations are related to large-scale changes in the electrostatic environment. The link to the commonly observed shorter scale fluctuations here (several micrometer scale) is not entirely clear.

Figure 2c graphs the time evolution of the brightness of the entire tube (black), the bottom bright segment (red), and the middle bright segment (blue). The overall trend, as we previously reported for blinking nanotubes, is exponentially down and with smaller segments showing much larger fluctuations.[3] We have therefore also plotted essentially resolution-limited spots of 1.1 μm (2 pixels) long from the bottom bright segment (blue) and middle bright segment (cyan). Cognet *et al.* working with short, acid-treated nanotubes in solution saw similar jumps and recognized that, in their case, they are stepwise.[4] Such stepwise jumps are also easily discerned here if a small enough segment of nanotube is examined (green, cyan). If the region of interest is on the order of 1 μm long, that is, comparable to exciton diffusion lengths, the stepwise quenching events are clear.

There are significant differences, however. As we will see more clearly later, before the stepwise plateaus are fully resolved in time, we see sudden jumps to these levels down and back up. In Figure 2c, in addition to stepwise jumps in luminescence intensity, one can also see sloped plateaus. For example, the cyan trace shows several gradual linearly increasing plateaus. More rapid decreasing segments can also be discerned in the same trace.

Figure 2d shows the evolution of the PL intensity with laser power. In this case, the traces were taken in decreasing laser power intensity. Also, fewer data points were taken per step, with typically 12 data points per laser power. The data come from the bright suspended segment at the bottom of Figure 2a, using a 3.3 μm long section. Blinking becomes significant above 10^{12} photons/s/μm^2, but apart from that, both the pristine and damaged nanotube show essentially linear scaling. A dotted line shows the linear fit, a solid line a power law fit; however, the two are so close as to be almost indistinguishable on the plot. The linear best fit is $y = (3.02 \pm 0.02) \times 10^{-6}x$, the marginally better power law fit is $y = (9 \pm 2) \times 10^{-6}x^{0.957\pm0.009}$. Any deviation from linearity is below the true experimental sensitivity. The red curve for the damaged tube is best fit by the linear $y = (1.07 \pm 0.01) \times 10^{-6}$, a negligibly better power law fit is $y = (4 \pm 2) \times 10^{-7}x^{1.03\pm0.02}$, essentially converging to linearity. The two curves are plotted separately but are so close as to be indistinguishable on the graph. The net loss in quantum efficiency with damage here is only a factor of just under three.

This was not one of the brighter tubes. It seems quite possible that the brightest nanotubes suffer the greatest loss in quantum efficiency, perhaps because they are most closely resonant (for example with E_{22}). Resonant nanotubes would have higher exciton populations for a given laser power and so the greatest opportunity for damage at a given excitation power.

For reference, assuming a geometrical cross section of 1 nm, and the double-layer graphene absorption of 4% gives an estimate of $y = 4 \times 10^{-5}x$ for 100% quantum efficiency, or equivalently in its undamaged state, this tube would have 7.5% quantum efficiency. Here again, uncertainties in excitation power uniformity and in absorption cross section are large, and this cannot be definitive. However, once again, the undamaged nanotube has higher quantum efficiency, and damaged or undamaged it still shows essentially linear scaling.

Much more information can be obtained from imaging spectroscopy, which for a one-dimensional material is in essence "hyperspectral imaging", with spatial and spectral information along orthogonal axes. Figure 3 shows the spectral evolution which was typical of many tubes. The 100× objective was used with 0.4 s integration time. Incident power was 7.5 mW at 405 nm. Figure 3a shows the spatial image of the nanotube with several suspended segments visible. Figure 3b shows a spectrally resolved image of the same nanotube. Following the same general approach as ref 3, using the nanotube itself as the slit, a diffraction grating was used to diffract the light along the horizontal axis, so the horizontal axis is spectral and the

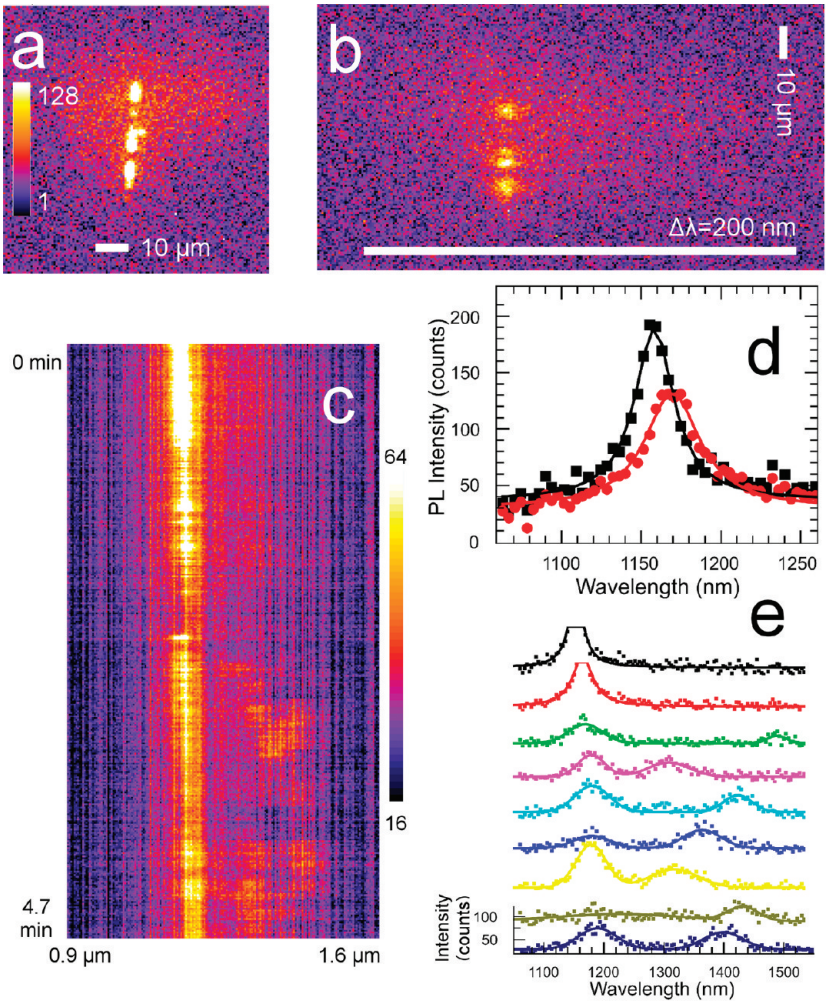

Figure 3. Spectral evolution with illumination. (a) Spatial image of suspended nanotube (color scale is in raw counts). (b) Imaging spectroscopy or "hyperspectral image" of the same tube. The *x*-axis is spectral, with long wavelength to the right. The *y*-axis is spatial, with the same scale as (a). (c) Spectral evolution of one segment of the nanotube, (d) slices of the tube PL spectrum at the beginning (black), just before the appearance of luminescent deep levels (red). The solid lines are Lorentzian fits. (e) Same two curves in black and red, and examples of the new deep levels that appear (other colors). The solid lines are Gaussian fits.

vertical axis is spatial with the same scale as in panel a. The spectral image shown is after 50 s exposure to the laser at the full power. It can be seen in Figure 3b that the nanotube is nearly uniform in terms spectral features, still emitting strong PL at E_{11}.

Figure 3c shows the time evolution of the average intensity of one of the spots. The full movie is included as Supporting Information. Spectral evolution over several minutes is shown. For the first half of the time, one can see that the PL peak weakens basically as in the previous examples. A small spectral shift can be barely discerned over this time; we return to it shortly. After 2 min, new bright levels are visible at long wavelengths.

Figure 3d shows the weakening and gradual spectral shift that occurs before the deep levels appear. This behavior is very generic, and we have seen it for many tubes. The initial E_{11} peak is fit by a Lorentzian centered at 1158.2 $\pm$ 0.5 nm. (The uncertainty quoted here and throughout assumes a given wavelength calibration. The actual uncertainty in the absolute calibration is larger.) After 70 s, before any deep levels are visible, the peak position has red-shifted to 1169.6 $\pm$ 0.7 nm. The peak broadens by 37% from a fwhm of 30 $\pm$ 1 to 41 $\pm$ 2 nm, and the integrated intensity falls by 6% in this time.

Figure 3e shows the same two peaks in black and red, and slices where deep levels were visible in other colors. The points are the original data, and the lines are Gaussian fits to the data. The deep levels are significantly broader than the E_{11} peak, with an average fwhm of 59 nm. The deep levels lie well below E_{11}. The separation in energy of the deep level is, in order from the green curve to the navy curve, 231, 105, 181, 143, 112, 188, and 156 meV. That is, it ranges from 105 to 231 meV. It is likely that there are longer wavelength deep levels for which our detection system is not sensitive.

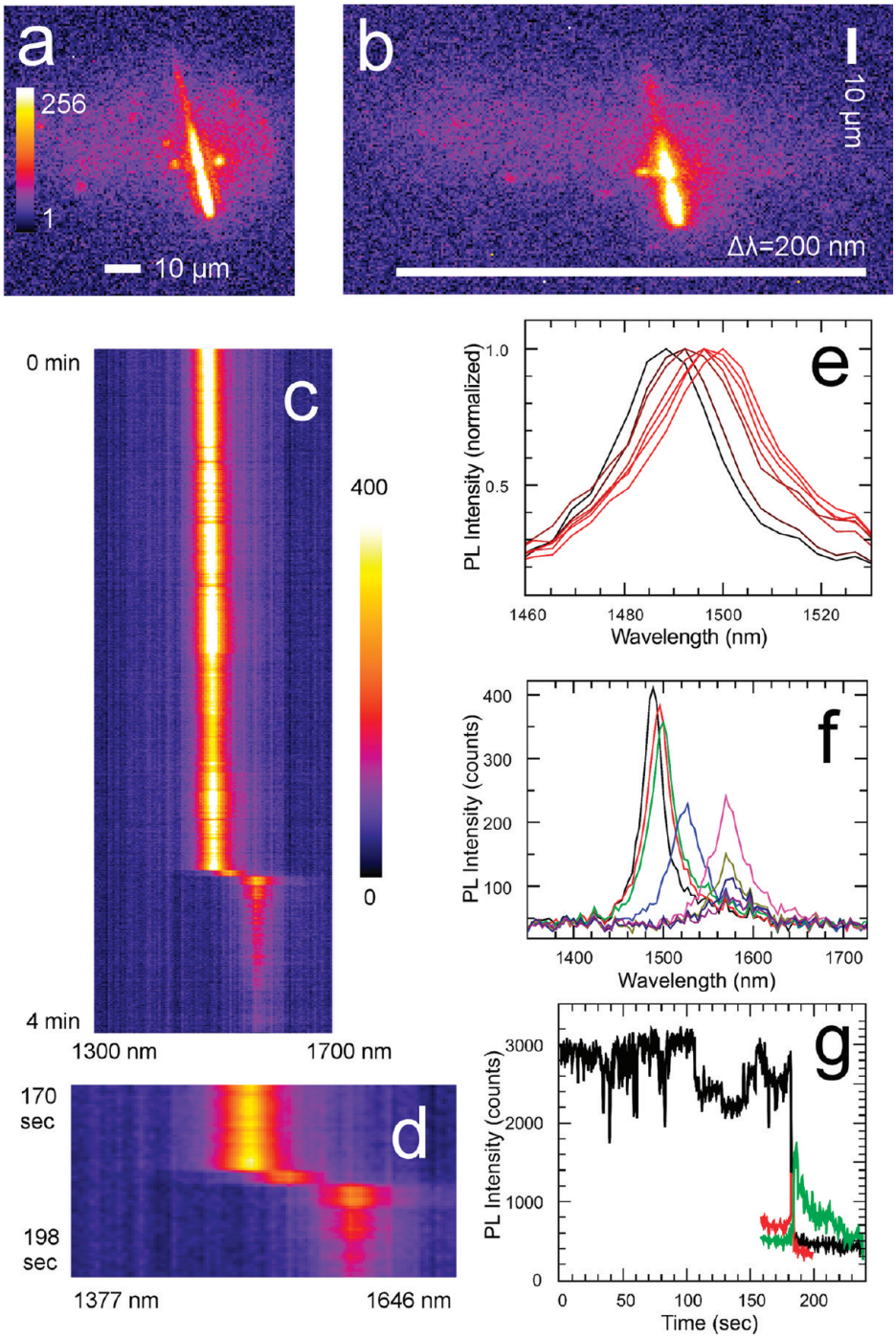

Figure 4. Unusual spectral evolution of a particular nanotube. (a) Spatial image of suspended nanotube. The catalyst stripe can be seen in the top half of the image, while the bottom part of the tube is over the catalyst free area. (The color scale is in raw counts.) (b) Imaging spectroscopy of the same nanotube. The *x*-axis is spectral, with long wavelength to the right. The *y*-axis is spatial with the same scale as (a). (c) Spectral evolution of one segment of the nanotube. (d) Close up on emergence of new levels. (e) Gradual shift and broadening of the PL peak as a function of time, before the appearance of the deep levels. (f) Initial peak (black), its time evolution (red, green), the transient peak (blue), and the final, decaying peak (pink, dark yellow, navy). (g) Time evolution of the E_{11} peak (black), the transient peak (red), and the final decaying peak (green).

Recently, there has been a great deal of interest in deep levels in nanotube PL. Early on in ensemble studies, ultraviolet (UV) radiation was shown to induce deep levels in the photoluminescence excitation (PLE) map.[14] The same sort of deep levels have been reported after UV exposure in a study of chirally purified tubes as well as single nanotubes, attributed to specific modes of oxygen chemisorption.[15] Nanotubes attacked by atomic hydrogen also show a level 40−80 meV below E_{11}.[16] In that case, the level was attributed to the brightening of dark excitons due to adsorption, as opposed to the creation of new dopant levels.

Nanotubes are thought to have spin-triplet dark excitons lying below the bright E_{11} singlet, and adsorbates might break the symmetry which formally forbids light emission from those states. Structure-dependent deep levels have been reported in the range of 0.1 to 0.2 eV for hole-doped nanotubes.[17] The insensitivity of the deep level to dopant type has led to the attribution of these deep levels to the X+ trion, which is a charged exciton consisting of two holes and one electron. Although they could not be created with low power cw excitation, deep levels were observed after exposing nanotubes to high pulse intensities.[5] In that case, deep levels (~0.19 eV) were attributed to photoinduced defect levels. Those levels seem consistent with what we see here.

Here, the levels are very deep, and the depth varies even for a single nanotube. The levels might loosely be grouped into three sets: one at ~0.10 eV, one at ~0.18 eV, and one at ~0.23 eV below E_{11}; however, the groups might also be coincidental. In any case, they are much deeper than any expected dark exciton but seem consistent with the idea of deep dopant levels. That they are spatially localized in most cases might be a hint that ionized fixed dopants are to blame, not free X+ trions; however, trions, because they are charged, would also be localized by any potential wells, and the spatial resolution is probably not high enough to exclude them on that basis alone.

Figure 4 shows similar data for another tube. This shows a somewhat similar evolution; however, this tube was atypical and very interesting in that the entire tube simultaneously hopped at two distinct times to new levels, which were shallower than the more typical ones like those above. The spatial image is shown in Figure 4a, using a 100× objective with 0.4 s integration time. The incident power was 2.85 mW at 405 nm. The catalyst area can be seen as a diffuse stripe on the top half of the image because of the abundant nanotubes there. The tube extends off the catalyst to the catalyst-free area at the bottom. Figure 4b shows the spectrally resolved image, this time at the full 7.5 mW. Longer wavelength is to the right. Because the tube is not vertical, the absolute spectral calibration is *y*-axis-dependent. The entire video is shown in Supporting Information.

Figure 4c shows the time evolution of the PL averaged over a 2.2 μm (4 pixel) long segment on the catalyst-free region. The PL is entirely stable for the first ~30 s and then begins fluctuating. After 182 s, the PL peak red shifts abruptly, and 2 s later, it red shifts again. The PL then fades away roughly exponentially at this fixed wavelength. Figure 4e shows the gradual red shift that occurs over the initial 182 s. The PL peaks are normalized to unity to emphasize only the shift, not the blinking, that occurs in the later stages. Each successive curve is 30 s apart, showing that the red shift is gradual and steady. Initially, the peak position, as determined

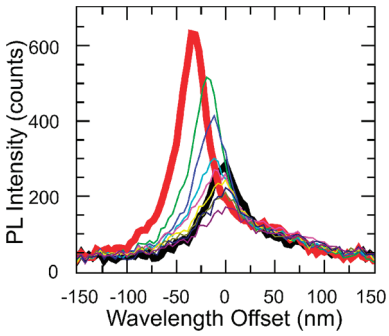

Figure 5. Unique blue shifting event observed. The initial PL peak is in black. The absolute wavelength is not calibrated, so the scale is centered at the center of the initial E_{11}. After 34 s illumination, the peak underwent a sudden band gap shift transition, blue shifting to the red curve. Subsequent curves at 1 min intervals show the gradual red shift, broadening, and slight decay in PL intensity (green, blue, cyan, magenta, yellow, navy, violet), nearly matching and eventually surpassing the original peak position.

by a Lorentzian fit, is 1488.5 ± 0.2 nm with a width of 27.8 ± 0.5 nm. By 180 s, just before the onset of the transition to the deep levels, the peak has shifted to 1499.6 ± 0.3 nm with a width of 36.8 ± 0.7 nm. The PL peak position shifts by 62 pm/s.

Figure 4f shows the spectral shift. The initial PL spectrum is in black. The red and green curves are 90 s intervals. The blue curve shows the transient peak, with a Lorentzian fit yielding 1526.0 ± 0.4 nm center and 47 ± 1 nm width. The magenta curve shows the final deep level, with a Lorentzian fit yielding 1572.0 ± 0.4 nm center and an unchanged 47 ± 1 nm width. The dark yellow curve is 10 s later, and subsequent curves are at 20 s intervals. The transient level then is about 14 meV below E_{11}, while the final level is about 38 meV below E_{11}.

Figure 4g shows the time evolution of the original E_{11} peak in black, the transient peak in red, and the final deep level in green. The wavelength integrated intensity averaged over a 2.2 μm (4 pixel) long segment is shown. The PL intensity is seen to be steady at the 10% level for the first 30 s, after which sudden downward spikes appear. After about 10 s, these downward spikes become resolved into plateaus that are basically just like the "stepwise quenching" of ref 4. In contrast with this reference, there is no exposure to acid but only exposure to a continuous wave laser, and yet it behaves very much like a nanotube which has been attacked by a single molecule quencher. This is similar to the oxygen ambient PL of ref 7. Finally, the E_{11} peak jumps to the transient level and then to the deep level. This deep level decays away nearly exponentially. Any jumps to deeper levels would likely be invisible to us because of the loss of detector sensitivity at still longer wavelengths.

Returning to gradual shift seen in the initial stages, one experiment was uniquely instructive, though unfortunately we have not been successful so far at

reproducing it. We once observed an SWNT undergo a sudden blue shift before the gradual red shift. The spectral data are shown in Figure 5, and the video is included in the Supporting Information. Regrettably, the wavelength was not absolutely calibrated, but each pixel corresponds to approximately 3.85 nm, with long wavelength to the right. We therefore plot the wavelength of the spectrum relative to the initial center of the peak at 0 nm. The initial peak (thick black line) wavelength was not determined, but it lies in the near-infrared band (~1.0 to 1.6 μm). These data were taken with the 100× objective at full power with about 7.5 mW 405 nm incident on the sample and a 400 ms integration time. This is a very bright tube, with per unit length brightnesses on par with the very bright tube shown in Figure 1. After 34 s illumination, the spectrum abruptly blue shifts 32 ± 1 nm (thick red line) and brightens by a factor of 1.80 ± 0.07 based on Lorentzian fits to the peak position and area. Subsequent illumination causes the peak to gradually red shift back and return to lower intensities. Each successive curve in Figure 5 is shown at 1 min intervals. After 3−4 min, the peak looks similar in intensity and brightness to how it looked initially. The peak continues to red shift, weaken, and broaden as time goes on.

DISCUSSION

Next we discuss the origin of these effects. First we consider the small, gradual red shift that occurs before the onset of any blinking or deep levels. The red shift is reminiscent to the sudden blue shift (~30 meV) we call the band gap shift transition (BST) which occurs when nanotubes are heated enough to desorb atmospheric adsorbates.[18] This transition has also been observed for intentionally ethanol-adsorbed nanotubes.[19] The fact that the nanotube in Figure 5 first underwent a blue shift of a similar magnitude to the BST, followed by gradual red shift which nearly overlaps and ultimately surpasses the original peak, suggests that the blue and red shifts arise from similar mechanisms. The nanotube initially heats up enough to desorb adsorbates, and the reduction in effective dielectric constant causes a blue shift. The red shift would then occur as the nanotube accreted atmospheric adsorbates. We shall argue below that this is not a passive process, but that it is actually active. However, first we shall discuss other evidence of reactions with adsorbates in the blinking data.

As seen above, short segments of nanotubes showed the same kind of stepwise jumps in PL intensity described in detail in ref 4. In their case, the jumps were induced by intentionally chemically attacking the nanotube by the addition of acids which protonated the nanotube locally. Here, the nanotube is always in the same ambient, in air, at atmospheric pressure, and we have not altered the atmospheric composition. The stepwise blinking is perhaps a bit surprising, then, and certainly is if one has in mind an idealized pristine nanotube sitting in perfect vacuum. The simplest explanation is that the stepwise blinking is exactly the same phenomena, molecular adsorption, but in this case, it is molecular adsorption from the ambient gas atmosphere. A possible culprit is gaseous oxygen, which can be highly reactive, in particular in singlet form. The presence of oxygen is known to quench nanotube PL in solution,[20] and oxygen has the effect of p-doping,[21] and in general, it is responsible for the degradation of many organic materials. Recent work has indicated that oxygen and water work in tandem to p-dope nanotubes,[22] and electrostatic doping has also been shown to cause the loss of PL.[23] Importantly, freely suspended nanotubes are reported to show photoluminescent blinking in oxygen ambient, but not in inert gases.[7] Blinking induced by intense illumination of micelle-encapsulated nanotubes on mica and glass was attributed to oxygen chemisorption.[5]

There are additional features in the blinking which are not readily explained in terms of static molecular quenchers adsorbing or desorbing as proposed in ref 4. For example, in Figure 4g, before new stepwise levels become clearly defined, there are spikes down and back up to the stepwise level. Rather than adsorbates adsorbing at the appearance of the spike and then desorbing, it seems more likely that the adsorbate binds at the initial spike, but it is quickly filled or screened by neighboring charge. The dopant may still be present, but the brightness spikes back up because charge fills the level or otherwise screens it. The spikes would evolve into plateaus as time goes on, and more adsorbates bind, further doping the tube, making it less able to screen or fill the new charge states.

The sloped segments of the stepwise plateaus seen in Figure 2c are also difficult to understand on the basis of adsorption and desorption alone, but they might be understandable in terms of changes in the local electrostatic environment.

The appearance of deep levels is related to the blinking. Processes expected to give rise to deep levels include brightening of dark excitons, trions, or other charged excitons and the introduction of dopant or defect states. Dark excitons are electron−hole pairs with symmetries for which optical recombination is forbidden to first order such as spin-triplets. Other perturbations might break that symmetry. However, the deep levels here are very deep, and the dark exciton is thought to be shallow, so this does not seem to be the best explanation. The trion is a three particle quasi-particle. The positive trion consists of two holes and one electron and has been reported for SWNTs, with hole doping inducing a trion at a specific deep level below E_{11} in that case.[17] However, here we have many levels, so they cannot be assigned to the trion, or at least they would have to represent various states of

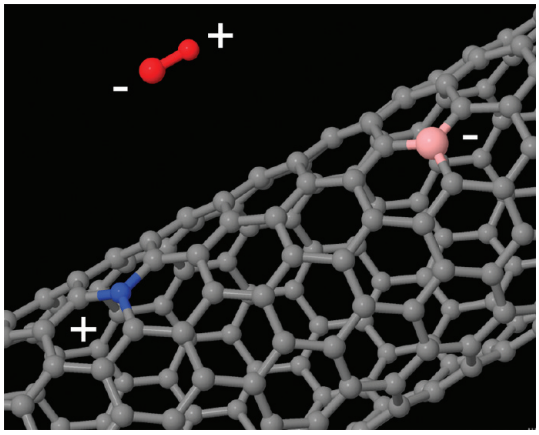

Figure 6. Schematic of the interaction between excitons and molecules. A single nanotube is illustrated in gray. An exciton consists of an electron and hole displaced, here illustrated schematically at one instant as a positively charged site in blue and a negatively charged site in pink. This has a dipole moment, represented by the "+" and "−" which interacts with molecules in the environment. A neutral oxygen molecule is illustrated in red. The excitonic dipole causes charge to reconfigure on the neutral molecule, inducing a dipole, represented by the "−" and "+". The molecule is attracted to the nanotube *via* this interaction.

charged excitons. Finally, defect states are blamed by others for deep levels.[6,14,15] Defect states typically lead to doping, and doping has been observed experimentally to quench PL.[4,20,23] Theoretical explanations for such quenching have been proposed.[24,25] Moreover, defect-induced quenching is used to understand how the excitonic quantum efficiency drops with doping in diffusion-limited contact quenching models.[26] Certainly doping is well-established in bulk semiconductors to introduce new optical levels. For all of these reasons, doping or defect-related states seem the most likely explanation for the deep levels here.

The blinking phenomena that preceed the overt appearance of deep levels might be explained also by the gradual introduction of dopants which, if they are present in very low concentrations, would provide a spatially nonuniform pathway for excitonic recombination, as in diffusion-limited contact quenching.[26] If the levels are sufficiently sparse, they are like buckets which can become full, and so invisible, leaving the tube bright, only to empty and become quenchers again. Rather than the adsorption and desorption of dopants, it is likely that much of the blinking and its onset stem initially from the introduction of dopant levels which fluctuate in terms of their charge state and so become hidden and revealed alternately. That is, a dopant may remain present, but its effect will depend on how mobile charge surrounds it. It can be filled completely or screened out if the charge environment permits. One can view the energy level structure as a kind of waterfall, with excitons diffusing from the highest E_{11} levels into defect states which fill and empty, leading to variations in the state filling of all levels.

How could illumination induce adsorption and these effects? Here we propose an explanation. While we tend to consider the electromagnetic field environment internal to the nanotube, nanotubes are inherently intimately connected with their environment. Changes to charge distribution within nanotubes cause changes to the electromagnetic field well outside of the nanotube. The environment is not static but responds to those changes. When the nanotube is optically excited, it generates excitons, which are electron−hole pairs. Another way to look at this is that electrons and holes which are displaced from one another are dipoles. It is well-known that the presence of a dipole polarizes neutral molecules, inducing an opposing dipole and that opposing dipoles are attractive, drawing them toward and helping them stick to the nanotube. A schematic figure of this interaction is shown in Figure 6. This type of interaction is a van der Waals force and is very strongly inverse in distance. Indeed, we have seen that such induced dipole forces can be strong enough to cause nanotubes to crash into a surface;[27] we have also seen how charge on the nanotube can induce charge polarization and redistribution on the nearby surface around it with visible consequences in SEM.[28]

If one considers the exciton as an "instantaneous" dipole, and if the interaction is with an induced dipole, for example, induced on a neutral oxygen molecule, the interaction would be considered a London dispersion force.[29] Any optically induced dipole would also interact with intrinsically dipolar molecules such as water, yielding dipole−dipole interaction which would be strong but also depend on the polarizability (the ability of permanent dipole to respond to the time variation of the excitonic dipole) of the molecule at the exciton frequency.

Such a model seems to explain the observed effects on the spectrum. On any surface, gas molecules from the atmosphere will be adsorbing and desorbing all of the time. In the absence of any external perturbation, the surface coverage will tend toward an equilibrium. The excitonic dipole attracts additional molecules through dipole−dipole interactions. These attracted molecules accrete on the surface of the nanotube. The photoinduced excitonic dipole can increase the collision frequency (collisional cross section), and it can increase the sticking coefficient.

Elementary thermodynamical and statistical physics considerations enable a quantitative estimate of the energy scales and time scales involved. Adsorbates which are physisorbed on nanotubes can be desorbed by moderate heating, thus binding energies must be of order the thermal energy, k_BT, where k_B is Boltzman's constant and T is the temperature in Kelvin. At 20 °C, this corresponds to 25 meV. For an ideal gas, $P = nk_BT$,

where P is the pressure and n is the molecular density, and so at atmospheric pressure and temperature, n is 4×10^{26} molecules/m^3, which corresponds to one molecule in each cube 3.4 nm on a side, on average in the gas phase.

Although the true situation is highly dynamic, the magnitudes of the electromagnetic interactions can be estimated in a static picture. The instanteous spatial separation of the electron and hole in an exciton is believed to be about 1 nm.[30] (The exciton diffusion length is much larger.) The dipole moment for point particles is the charge multiplied by the separation, so the instantaneous dipole moment for the exciton can be estimated to be p_X = (1 nm)e, where e is the elementary charge. Consider the magnitude of induced dipole that would result in a 50% (*i.e.*, of order 13 meV) change in the binding energy. Neglecting factors of order unity, dipole−dipole interaction potential energies are of order $U = p_1 p_2/4\pi\varepsilon r^3$, where p_1 and p_2 are the dipole moments, ε is the permittivity, and r is the interdipole spacing. Using the free space permittivity, assuming a separation r = 1 nm, and using the above dipole moment, a 50% change in binding energy is induced by a dipole moment of (0.01 nm)e. This charge displacement is small and appears reasonable when compared to the van der Waals radius of 0.15 nm for O_2, on the order of 10 times higher.

Stepping slightly away from this fully static picture, we can estimate that an exciton in a nanotube at atmospheric temperature and pressure has one collision with an atmospheric molecule in its lifetime. From kinetic theory, the impingement rate of nitrogen at atmospheric pressure and near room temperature is 3×10^{23} molecules/cm^2/s.[31] For the graphene density of 38 carbon atoms/nm^2, this corresponds to one molecular collision with each carbon atom every 10 ns. For a diameter d = 0.7 nm nanotube, along the length of order l = 1 nm defining the exciton at any given instant, this corresponds to a collision with the surface area πdl = 2.2 nm^2 every 150 ps. This is the same magnitude as the radiative lifetime in single-walled carbon nanotubes. This not only indicates the availability of molecules for photoinduced adsorption but also points to molecular collisions as a source of broadening and as a significant factor in the exciton lifetime of air-suspended carbon nanotubes.

In the context of this simple picture, it is also straightforward to show that the trajectories of atmospheric molecules can be altered by interactions with the excitonic dipole. An extreme case is when the excitonic dipole actually captures a gas-phase-induced dipole. An average atmospheric gas molecule has kinetic energy K of $K = k_B T$ (up to a small factor of order unity). Using an excitonic dipole p_X = (1 nm)e and supposing an induced dipole of p_I = (0.01 nm)e, the potential energy U is the same as the kinetic energy K for a separation of r = 0.8 nm. This indicates that an average molecule that can be at least that polarized should be captured by the exciton if it approaches within 0.8 nm of it. This should be common at atmospheric pressure and temperature.

The induced dipoles should have predictable effects on the spectrum, as well. Since they oppose the excitonic dipole, they would tend to reduce the magnitude of the dipole and so reduce the PL peak intensity. However, such effects may not be so clear since changes in the PL intensity are also possible due to the shift in absorption peak wavelengths that result from dielectric screening. Second, because the interaction is attractive, they should shift the peak toward longer wavelength. This is a microscale picture of dielectric screening which is used to understand how PL peaks shift in response to changes in their dielectric environment. The broadening effect seems to share the characteristics with what in molecular spectroscopy is called "van der Waals broadening" in both the magnitude and direction of the observed shift.[32]

The appearance of deep levels seems to fit into this dipole-induced molecular deposition picture, as well, if one supposes that occasionally a molecule that comes in contact with the nanotube transfers charge to it, for example, *via* covalent bonding. This could occur if the molecule is in the vicinity of a region where the nanotube is in a highly excited state, for example, in a state like E_{11}, or it could occur if a highly reactive molecule contacts the nanotube, for example, singlet oxygen, which is well-known to quench the PL of many organic fluorophores. This process likely occurs without illumination, but it could be greatly enhanced with illumination. There would be continuous physisorption of molecules which causes the dipole-induced red shift and simultaneous chemisorption of dopants which introduce the deep levels, which ultimately radically alters the PL spectra.

Physisorption may be more common than chemisorption simply due to greater atmospheric abundance of relatively nonreactive molecules. Photons through dipole−dipole interaction would then increase the impingement rate on the nanotube. However, photons could play a more active role and be responsible for the conversion of molecules from weakly perturbing physisorbed admolecules into more reactive molecules (which would chemisorb and be responsible for deep levels). There are at least two distinct pathways whereby light could cause chemisorption instead of physisorption: one when the nanotube reactivity is enhanced through photoexcitation and the other when the molecule is photoexcited to a reactive excited state. The first path seems quite possible since the exciton can be viewed as derived from an antibonding state and hence should be more reactive. Also, singlet and triplet excitons are thought to be present in nanotubes, and the presence of various excitonic spin states might facilitate such reactions.

As discussed in ref 5, optically excited SWNTs might transform oxygen into singlet oxygen, which would be likely to chemisorb.[33] The second path seems possible as well, but the absorption cross section (optical) for single molecule excitation is small and should depend strongly on excitation energies. Photons could, for example, convert triplet oxygen into singlet oxygen. Under the low excitation power density in these experiments, we believe that the direct excitation of oxygen and other molecules into highly reactive states is likely not very significant.

Regardless of the mechanism, a practical outcome of this work is the ability to use moderate light intensities to modulate the band gap of the nanotube locally, producing a true one-dimensional heterostructure. Modulations of the magnitude of about 30 meV can be made the scale of the wavelength of the violet light used here (405 nm) without serious loss of luminescence intensity. In more macroscopic terms, this is a very high field of 0.7 kV/cm. This provides a way to perform band gap engineering on carbon nanotubes.

The dipole-induced molecular deposition concept should enable interesting new ways to controllably alter nanotubes. We tend to view the nanotube surface as relatively inert. However, optical excitation provides a tool to actively induce interactions between the nanotube and its environment and to make the nanotube chemically more reactive.

CONCLUSION

In conclusion, we have shown how bright air-suspended luminescent SWNTs undergo a series of changes even at relatively low illumination intensities. Changes include spectral red shifts of 10s of meV, blinking, dramatic loss of quantum efficiency, and the appearance of new deep levels. The pristine nanotube has high quantum efficiency, while the photodamaged nanotube does not. To explain the evolution of the spectral features, we introduce a light-induced molecular deposition picture, based on attractive forces between the exciton and the dipole moment of molecules in the surrounding environment, causing locally enhanced physisorption and chemisorption. This work is useful as an approach to locally engineer the band gap and defect densities along the nanotube.

METHODS

Sample Preparation. SWNTs were grown by water-assisted atmospheric pressure acetylene chemical vapor deposition (CVD) in a cold-walled CVD reactor. Cobalt thin film was used to seed the nanotube synthesis.

Substrates were photolithographically patterned quartz gratings with varying spacings on the order of 5 μm and nominal depth of 0.2 μm. Quartz was chosen as a substrate because of its transparency and very low background fluorescence, in contrast to silicon substrates, which are commonly used.

Optical Setup. Videos were made of the spatially and spectrally resolved PL of extended (>10 μm) SWNTs, with a setup similar to our prior work.[3] Here, illumination was with a 50 mW violet (405 nm) laser. After passing through the optical system 4−8 mW was incident on the sample. The power was varied by interrupting the beam with two neutral density filters on filter wheels with optical effective densities ranging from 0.08 to 2.5. Spectrally resolved images were obtained by using the nanotube itself as the slit and diffracting the collimated light off a 45 lines/mm reflection grating, as in ref 3. Here microscope objectives of 100× (NA 0.7) and 160× (NA 0.95) were used to collect the emission. Excitation was through these same objectives, using a 50 mm lens to defocus the spot, resulting in 60 and 54 μm diameter illuminated spots, respectively. Integration times of 200 to 400 ms were used to give strong signal-to-noise ratios even at low excitation powers. (Bright air-suspended nanotubes are routinely visible with integration times on the order of 1 ms.) All observations were in ambient conditions, in room air, and at room temperature.

Laser Power Sweeps. To vary the incident power, the laser power was fixed but passed through a neutral density filter wheel with a double stack of filters. The 405 nm laser was 50 mW full power passed through a depolarizer and the filter wheel through a defocusing lens and 45° dichroic beam splitter. The lowest excitation powers used filter OD 2.5, and the highest powers used filter OD 0.08. In Figure 1, the nanotube was excited and imaged through the 160× objective with a ~54 μm diameter spot. With this objective, at full power, the incident power on the sample was 4.4 mW. For each filter combination, the data were taken for several seconds, amounting to dozens of data points for each laser power. Figure 1a shows the segment at the second highest power (filter OD 0.14). It is very bright, with peak intensities of nearly 6000 ADU (analog to digital units) counts with 200 ms integration; however, it has already sustained some damage by this point. For this objective, 1 ADU count corresponded to 65 photons, so peak PL intensities are 2×10^6 photons/s/pixel.

The tube segment measured in Figure 1c was 5.3 μm long. At this magnification, 1 μm corresponds to 2.8 pixels. To go from detected photons to integrated photons, it was assumed that the emission was isotropic. The 160× objective has NA 0.95, so scaling that isotropically to 4π steradians results in a factor of 2.9. More realistic would be to use a dipole radiation pattern, which introduces a cosine factor that would slightly reduce the correction factor. To go from incident photons to photons/unit area, it was assumed that the illumination intensity was uniform across the entire spot. This is only an approximation since the diode produces an elliptical beam and the optical system distorts it in several ways. Moving the nanotube across the field leads to increases and decreases in intensity of approximately a factor of 5. This illumination nonuinformity is the main source of error in the absolute excitation intensities.

For the tube segment in Figure 2d, a 100× objective with NA 0.7 was used, and scaling isotropically to 4π results in a correction factor of 6.8. It was assumed that the illumination was uniform across the 60 μm diameter spot. Again, this is the largest source of error and leads to an overestimate of the quantum efficiency. For this objective, the calibrated response of the system was 100 photons/ADU count. The integration time was 400 ms. Thus, for reference, peak brightnesses of 1000 counts/pixel correspond to collected photon fluxes of 2.5×10^5 photons/s/pixel, which with the isotropic correction factor becomes 1.7×10^6 photons/s/pixel. There are 1.82 pixels/μm here.

Fits. In Figure 1c, the dotted black line is a linear fit, with best fit $y = (7.02 \pm 0.07) \times 10^{-5}x$ giving a statistical R^2 of 0.93. The solid black line is a power law, with best fit $y = (0.009 \pm 0.003)x^{0.81\pm0.01}$

giving a statistical R^2 of 0.96. The dotted red line is a linear fit, with best fit $y = (4.16 \pm 0.03) \times 10^{-6}x$ giving a statistical R^2 of 0.972. The solid red line is a power power law $y = (2.9 \pm 0.9) \times 10^{-5}x^{0.92\pm0.01}$ giving a statistical R^2 of 0.976. All fits were computed with the open source program QtiPlot.

In Figure 2d, the dotted black line is a linear fit, with best fit $y = (3.02 \pm 0.02) \times 10^{-6}x$ giving a statistical R^2 of 0.989. The solid black line is a power law, with best fit $y = (9 \pm 2) \times 10^{-6}x^{0.957\pm0.009}$ giving an only marginally better R^2 of 0.990. Two lines are plotted in red; however, they overlap so completely as to be indistinguishable on this scale, and any deviation from linearity is below the true experimental sensitivity. The dotted red line is a linear fit with best fit $y = (1.07 \pm 0.01) \times 10^{-6}x$ with an R^2 of 0.9602. The solid red line is a power law $y = (4 \pm 2) \times 10^{7}x^{1.03\pm0.02}$ with an R^2 of 0.9607.

Quantum Efficiency. For the pristine tube, emitting on the order of 10^{-4} photons/μm per photon incident in a μm^2 necessary implies a high quantum efficiency. The tube diameter is approximately 1 nm and is much longer than 1 μm in length, so if it had 100% capture cross section, one would expect 1 photon in 10^3 captured. However, the nanotube is so thin that only ~1% is expected to be absorbed. Early experimental data put the cross section near 0.5%,[34] though more recent data, such as that from graphene, indicate it is higher. Assuming the tube is like a graphene double layer with $2\pi\alpha = 4\%$ absorption[11] leads to an expectation of 4×10^{-5} photons emitted per/μm for photons incident on 1 μm^2 assuming the quantum efficiency internal to the nanotube is unity. This is less than the measured value. However, the nonuniformity in excitation intensity is a significant source of error. Also, the absorption cross section at 405 nm may be higher. Still, the quantum efficiency cannot be low.

Conflict of Interest: The authors declare no competing financial interest.

Acknowledgment. We are grateful to Paul Marshall for nanotube growth, Hue Tran and Mike Denhoff for catalyst deposition, and Sylvain Laframboise, Philip Waldron, and Mathew Shiu for quartz grating patterning.

Supporting Information Available: Videos of a nanotube in stable and blinking states. Video of a very large scale blinking nanotube. Title slide for these videos with scales. Videos corresponding to Figures 3, 4, and 5. This material is available free of charge *via* the Internet at http://pubs.acs.org.

REFERENCES AND NOTES

1. Htoon, H.; O'Connel, M. J.; Cox, P. J.; Doorn, S. K.; Klimov, V. I. Low Temperature Emission Spectra of Individual Single-Walled Carbon Nanotubes: Multiplicity of Subspecies within Single-Species Nanotube Ensembles. *Phys. Rev. Lett.* **2004**, *93*, 027401-1–027401-4.
2. Matsuda, K.; Kanemitsu, Y.; Irie, K.; Saiki, T.; Someya, T.; Miyauchi, Y.; Maruyama, S. Photoluminescence Intermittancy in an Individual Single-Walled Carbon Nanotube at Room Temperature. *Appl. Phys. Lett.* **2005**, *86*, 123116-1–123116-3.
3. Lefebvre, J.; Austing, D. G.; Bond, J.; Finnie, P. Photoluminescence Imaging of Suspended Single-Walled Carbon Nanotubes. *Nano Lett.* **2006**, *6*, 1603–1608.
4. Cognet, L.; Tsyboulski, D. A.; Rocha, J.-D. R.; Doyle, C. D.; Tour, J. M.; Weisman, R. B. Stepwise Quenching of Exciton Fluorescence in Carbon Nanotubes by Single-Molecule Reactions. *Science* **2007**, *316*, 1465–1468.
5. Georgi, C.; Hartman, N.; Gokus, T.; Green, A. A.; Hersam, M. C.; Hartschuh, A. Photoinduced Luminescence Blinking and Bleaching in Individual Single-Walled Carbon Nanotubes. *Chem. Phys. Chem.* **2008**, *9*, 1460–1464.
6. Harutyunyan, H.; Gokus, T.; Green, A. A.; Hersam, M. C.; Allegrini, M.; Hartschuh, A. Defect-Induced Photoluminescence from Dark Excitonic States in Individual Single-Walled Carbon Nanotubes. *Nano Lett.* **2009**, *9*, 2010–2014.
7. Yoshikawa, K.; Matsuda, K.; Kanemitsu, Y. Exciton Transport in Suspended Single Carbon Nanotubes Studied by Photoluminescence Imaging Spectroscopy. *J. Phys. Chem. C* **2010**, *114*, 4353–4356.
8. Ai, N.; Walden-Newman, W.; Song, Q.; Kalliakos, S.; Strauf, S. Suppression of Blinking and Enhanced Exciton Emission from Individual Carbon Nanotubes. *ACS Nano* **2011**, *5*, 2664–2670.
9. Siitonen, A. J.; Bachilo, S. M.; Tsyboulski, D. A.; Weisman, R. B. Evidence for Long-lived, Optically Generated Quenchers of Excitons in Single-Walled Carbon Nanotubes. *Nano Lett.* **2012**, *12*, 33–38.
10. Crochet, J. J.; Duque, J. G.; Werner, J. H.; Doorn, S. K. Photoluminescence Imaging fo Electronic Impurity-Induced Exciton Quenching in Single-Walled Carbon Nanotubes. *Nat. Nanotechnol.* **2012**, http://dx.doi.org/10.1038/nnano.2011.227.
11. Nair, R. R.; Blake, P.; Grigorenko, A. N.; Novoselov, K. S.; Booth, T. J.; Stauber, T.; Peres, N. M. R.; Geim, A. K. Fine Structure Constant Defines Visual Transparency of Graphene. *Science* **2008**, *320*, 1308–1308.
12. Ju, S.-Y.; Kopcha, W. P.; Papadimitrakopoulos, F. Brightly Fluorescent Single-Walled Carbon Nanotubes *via* an Oxygen-Excluding Surfactant Organization. *Science* **2009**, *323*, 1319–1323.
13. Lee, A. J.; Wang, X.; Carlson, L. J.; Smyder, J. A.; Loesch, B.; Tu, X.; Zheng, M.; Krauss, T. D. Bright Fluorescence from Individual Single-Walled Carbon Nanotubes. *Nano Lett.* **2011**, *11*, 1636–1640.
14. Iakoubovskii, K.; Minami, N.; Kim, Y.; Miyashita, K.; Kazaoui, S.; Nalini, B. Midgap Luminescence Centers in Single-Wall Carbon Nanotubes Created by Ultraviolet Illumination. *Appl. Phys. Lett.* **2006**, *89*, 173108-1–173108-3.
15. Ghosh, S.; Bachilo, S. M.; Simonette, R. A.; Beckingham, K. M.; Weisman, R. B. Oxygen Doping Modifies Near-Infrared Band Gaps in Fluorescent Single-Walled Carbon Nanotubes. *Science* **2010**, *330*, 1656–1659.
16. Nagatsu, K.; Chiashi, S.; Konabe, S; Homma, Y. Brightening of Triplet Dark Excitons by Atomic Hydrogen Adsorption in Single-Walled Carbon Nanotubes Observed by Photoluminescence Spectroscopy. *Phys. Rev. Lett.* **2010**, *105*, 157403-1–157403-4.
17. Matsunaga, R.; Matsuda, K.; Kanemitsu, Y. Observation of Charged Excitons in Holed Carbon Nanotubes Using Photoluminescence and Absorption Spectroscopy. *Phys. Rev. Lett.* **2011**, *106*, 037404-1–037404-4.
18. Finnie, P.; Homma, Y.; Lefebvre, J. Band-Gap Shift Transition in the Photoluminescence of Single-Walled Carbon Nanotubes. *Phys. Rev. Lett.* **2005**, *94*, 247401-1–247401-4.
19. Chiashi, S.; Watanabe, S.; Hanashima, T.; Homma, Y. Influence of Gas Adsorption on Optical Transition Energies of Single-Walled Carbon Nanotubes. *Nano Lett.* **2008**, *8*, 3097–3101.
20. Dukovic, G.; White, B. E.; Zhou, Z.; Wang, F.; Jockusch, S.; Steigerwald, M. L.; Heinz, T. F.; Friesner, R. A.; Turro, N. J.; Brus, L. E. Reversible Surface Oxidation and Efficient Luminescence Quenching in Semiconductor Single-Wall Carbon Nanotubes. *J. Am. Chem. Soc.* **2004**, *126*, 15271–15276.
21. Collins, P. G.; Bradley, K.; Ishigami, M.; Zettl, A. Extreme Oxygen Sensitivity of Electronic Properties of Carbon Nanotubes. *Science* **2000**, *287*, 1801–1804.
22. Levesque, P. L.; Sabri, S. S.; Aguirre, C. M.; Guillemette, J.; Siaj, M.; Desjardins, P.; Szkopek, T.; Martel, R. Probing Charge Transfer at Surfaces Using Graphene Transistors. *Nano Lett.* **2011**, *11*, 132–137.
23. Ohno, Y.; Kishimoto, S.; Mizutani, T. Photoluminescence of Single-Walled Carbon Nanotubes in Field-Effect Transistors. *Nanotechnology* **2006**, *17*, 549–555.
24. Kinder, J. M.; Mele, E. J. Nonradiative Recombination of Excitons in Carbon Nanotubes Mediated by Free Charge Carriers. *Phys. Rev. B* **2008**, *78*, 155429-1–155429-8.
25. Perebeinos, V.; Avouris, P. Phonon and Electronic Nonradiative Decay Mechanisms of Excitons in Carbon Nanotubes. *Phys. Rev. Lett.* **2008**, *101*, 057401-1–057401-4.
26. Hertel, T.; Himmelein, S.; Ackermann, T.; Stitch, D.; Crochet, J. Diffusion Limited Photoluminescence Quantum Yields in 1-D Semiconductors: Single-Wall Carbon Nanotubes. *ACS Nano* **2010**, *4*, 7161–7168.

27. Kaminska, K.; Lefebvre, J.; Austing, D. G.; Finnie, P. Real-Time Global Raman Imaging and Optical Manipulation of Suspended Carbon Nanotubes. *Phys. Rev. B* **2006**, *73*, 235410-1–235410-7.
28. Finnie, P.; Kaminska, K.; Homma, Y.; Austing, D. G.; Lefebvre, J. Charge Contrast Imaging of Suspended Nanotubes by Scanning Electron Microscopy. *Nanotechnology* **2008**, *19*, 335202-1–335202-6.
29. http://en.wikipedia.org/wiki/Van_der_Waals_force.
30. Wang, F.; Dukovic, G.; Brus, L. E.; Heinz, T. F. The Optical Resonances in Carbon Nanotubes Arise from Excitons. *Science* **2005**, *308*, 838–841.
31. Hudson, J. B. *Surface Science: An Introduction*; John Wiley & Sons, Inc.: New York, 1992; p 137.
32. http://Physics.nist.gov/Pubs/AtSpec/node20.html.
33. Savage, T.; Bhattacharya, S.; Sadanadan, B.; Gaillard, J.; Tritt, T. M.; Sun, Y.-P.; Wu, Y.; Nayak, S.; Car, R.; Marzari, N.; Ajayan, P. M.; Rao, A. M. Photoinduced Oxidation of Carbon Nanotubes. *J. Phys.: Condens. Matter* **2003**, *15*, 5915–5921.
34. Islam, M. F.; Milkie, D. E.; Kane, C. L.; Yodh, A. G.; Kikkawa, J. M. Direct Measurement of the Polarized Optical Absorption Cross Section of Single-Wall Carbon Nanotubes. *Phys. Rev. Lett.* **2004**, *93*, 037404-1–037404-4.